Quaternary Geochronology xxx (xxxx) xxx–xxx

Contents lists available at ScienceDirect

Quaternary Geochronology

journal homepage: www.elsevier.com/locate/quageo

Luminescence age constraints on the Pleistocene-Holocene transition recorded in loess sequences across SE Europe

D. Constantin[a,*], D. Veres[a,b], C. Panaiotu[c], V. Anechitei-Deacu[a,d], S.M. Groza[a,d], R. Begy[a,d], S. Kelemen[a,d], J.-P. Buylaert[e,f], U. Hambach[g], S.B. Marković[h], N. Gerasimenko[i], A. Timar-Gabor[a,d]

[a] Interdisciplinary Research Institute on Bio-Nano-Science of Babeş-Bolyai University, Treboniu Laurian 42, 400271, Cluj-Napoca, Romania
[b] Romanian Academy, Institute of Speleology, Clinicilor 5, 400006, Cluj-Napoca, Romania
[c] University of Bucharest, Faculty of Physics, Atomiştilor 405, 077125, Măgurele, Romania
[d] Faculty of Environmental Sciences and Engineering, Babeş-Bolyai University, Fântânele 30, 400294, Cluj-Napoca, Romania
[e] Center for Nuclear Technologies, Technical University of Denmark, DTU Risø Campus, Roskilde, Denmark
[f] Nordic Laboratory for Luminescence Dating, Department of Geoscience, Aarhus University, Risø Campus, Roskilde, Denmark
[g] BayCEER & Chair of Geomorphology, University of Bayreuth, Universitätsstraße 30, 94450, Bayreuth, Germany
[h] Laboratory for Paleoenvironmental Reconstruction, Faculty of Sciences, University of Novi Sad, Trg Dositeja Obradovića 2, 21000, Novi Sad, Serbia
[i] Earth Sciences and Geomorphology Department, Taras Shevchenko National University of Kyiv, Glushkova Prospect 2a, 03127, Kiev, Ukraine

ARTICLE INFO

Keywords:
Loess
Luminescence dating
Magnetic susceptibility
Pleistocene-holocene transition
Southeastern europe

ABSTRACT

Here we investigate the timing of the last glacial loess (L1) - Holocene soil (S0) transition recorded in loess-paleosol sequences from SE Europe (Ukraine, Romania, Serbia) by applying comparative luminescence dating techniques on quartz and feldspars. Equivalent dose measurements were carried out using the single-aliquot regenerative-dose (SAR) protocol on silt (4–11 μm) and sand-sized (63–90 μm and coarser fraction when available) quartz. Feldspar infrared stimulated luminescence (IRSL) emitted by 4–11 μm polymineral grains was measured using the post IR-IRSL$_{290}$ technique.

The paleoenvironmental transition from the last glacial loess to the current interglacial soil was characterized using magnetic susceptibility and its frequency dependence. SAR-OSL dating of 4–11 μm, 63–90 μm and 90–125 μm quartz provided consistent ages in the loess-paleosol sites investigated, while the post-IR IRSL$_{290}$ protocol proved unreliable for dating such young samples. Based on these ages and the threshold of the magnetic signal enhancement the onset of soil formation has been placed around 16.6 ± 1.1 ka at Roxolany (Ukraine), 13.5 ± 0.9 ka at Mošorin (Serbia) and between 17.6 ± 1.4 ka and 12.4 ± 1.0 ka at Râmnicu Sărat (Romania). The trend observed in the magnetic parameters reflects the intensity of pedogenesis induced by regional climate amelioration during the Late Glacial, but the onset of magnetic susceptibility enhancement precedes the stratigraphic boundary of Pleistocene-Holocene dated at 11.7 ka in ice core records.

Thus, magnetic susceptibility indicates a gradual increase in pedogenesis after Termination 1 (~17 ka in the North Atlantic) at the sampling sites. Based on current data, it is not possible to define a synchronous threshold of change for all sections. However, the trend in the magnetic susceptibility data closely reflects the gradual transition from Last Glacial Maximum (LGM) towards the Holocene, with the onset of humus accumulation (A1 horizon) possibly linked to the prevalence of full interglacial conditions.

1. Introduction

The need for a better understanding of past environmental change has led to increasing efforts in improving chronologies for paleoclimate records worldwide (Blockley et al., 2012; Veres et al., 2013; Lisiecki and Raymo, 2005; Govin et al., 2015). For loess-paleosol sequences (LPS), as the most extensive paleoclimate archives on land, the issue is even more compelling, as in many cases the chronological control is often achieved only by matching and/or tuning to other records (Marković et al., 2015 and references therein). Loess is amenable to OSL dating as shown by previous studies (Roberts, 2008; Stevens et al., 2011, 2018).

It is generally assumed that dust deposition is enhanced during glacial times, whereas pedogenetic processes are stronger during warm-

* Corresponding author.
E-mail address: daniela.constantin@ubbcluj.ro (D. Constantin).

https://doi.org/10.1016/j.quageo.2018.07.011
Received 6 December 2017; Received in revised form 28 June 2018; Accepted 23 July 2018

wet climates, potentially those associated with interglacial periods (Maher et al., 2003). For LPS, the climatic transitions are recorded by changes in magnetic susceptibility; a proxy that solely reflects the strength of pedogenetic processes in cases where the parent loess is mineralogically homogenous. The magnetic susceptibility record in LPS is often wiggle matched or tuned to ice records or marine sediments proxies. This is based on the assumption that the climatic changes reflected in the terrestrial, marine or ice records are synchronous, at least at glacial-interglacial transitions (Marković et al., 2015 and references therein; Zeeden et al., 2018). For example, the transition between Late Glacial and Holocene dated at 11.7 ka ago based on the layer-counted GICC05 timescale (Rasmussen et al., 2014; Svensson et al., 2008) is probably the most easily identifiable. Moreover, this transition occurs over a time range that can be dated with numerous techniques. However, a recent study comparing radiocarbon records over the most recent deglaciation highlighted differences in the timing of the benthic $\delta^{18}O$ change in various marine records, globally (Stern and Lisiecki, 2014). If the synchronicity assumption does not hold even for the most recent glacial/interglacial transition, then the whole approach behind the magnetic and pedostratigraphic timescale tuning when linking loess chronologies, for example, to the marine isotopic time-series (Marković et al., 2015; Zeeden et al., 2018), must be reassessed.

In this study we have investigated three LPS that display a relatively rapid variation in their magnetic susceptibility records across the last glacial loess (L1) - Holocene soil (S0) transition. These three sites follow a transect in southeastern Europe, from the Dnieper river to the Carpathian Basin (Fig. 1). Our aim is to identify the onset of enhancement in the magnetic susceptibility record that in such records is commonly thought to reflect the Pleistocene/Holocene transition and to date it using multiple luminescence dating techniques.

2. Sampling and site descriptions

Luminescence samples were collected to bracket, as closely as possible, the transition between the loess (L1) and the Holocene soil (S0), as identified visually in the field. The L1/S0 transition was tentatively identified as the visual boundary between proper loess and the overlying humus rich (A1 horizon) S0 soil – the transitional zone would refer to the interval encompassing the genetic horizons (other than A1) of S0 that are clearly visible at all sites. The samples for OSL dating and magnetic measurement have been collected from the areas unaffected by syndepositional bioturbation, if this issue was identified at the sampling sites. Syndepositional bioturbation is not considered an issue in the luminescence dating studies because it usually affects hundreds of years of depositions, which are encompassed in the total errors of the OSL ages, which are around 1 ka for such young samples.

The Roxolany outcrop (46.2° N, 30.5° E) is situated on the left bank of the Dniester estuary, about 40 km southwest of Odessa, in southwestern Ukraine (Fig. 1 and Fig. S1). It is one of the most representative LPS in Eastern Europe (Nawrocki et al., 2018 and references therein), but limited investigations have been conducted on the L1/S0 transition. Seven luminescence samples were collected from the topmost 2.2 m, whereas samples for magnetic analysis were taken contiguously over 2 cm increments. The sequence consists of pale yellowish loess below ca. 95 cm depth, capped by a transitional horizon between 60 and 95 cm depth with increasing carbonate content towards the lower boundary. The upper part (0–50/60 cm depth) consists of a dark-grey to brownish chernozem soil.

The Râmnicu Sărat loess-paleosol (45.4° N, 27.0 °E; 160 m) sequence is located on the left bank of the Râmnicu Sărat river valley in central-eastern Romania (Fig. 1 and Fig. S2). In the field, the transition from L1 loess to S0 soil in terms of color change is gradual, spreading from 110 cm to 130 cm depth. Twelve luminescence samples have been collected from the topmost 1.6 m, closely encompassing the visual L1/S0 transition. Part of the material from each sample has also been used for magnetic analysis.

The Mošorin Veliki Surduk site (45.3° N and 20.2° E; 116 m) is located on the western slope of a 35 m deep gully, at the southern edge of Mošorin village on the Titel Loess Plateau, Vojvodina, Serbia (Fig. 1 and Fig. S3). Perić et al. (in press) reported a quartz OSL chronology for the upper last glacial cycle recorded at a site, located some tens of meters to the east of the one investigated in this study. The basal last glacial loess is very porous and in some parts intensively affected by syndepositional bioturbation. Many spherical, relatively soft carbonate nodules and humus infiltrations in old root channels are expressed at the contact zone with the Holocene soil. The S0 spans the upper 45 cm of the section with an upper steppic Ah horizon and a lower transitional AC horizon (the lowermost 15 cm) containing small soft spherical carbonate concretions (from 1 to 2 cm in diameter). Here, eleven OSL samples have been collected from the topmost 1 m. Sampling for magnetic analysis was carried out at 5 cm resolution.

3. Methods and instrumentation

3.1. Magnetic susceptibility

For samples collected from the Roxolany and Mošorin Veliki Surduk sections, the volumetric magnetic susceptibility was measured at frequencies of 300 Hz and 3000 Hz in a static field of 300 mA/m using a Magnon International VSFM (sensitivity $\sim 10^{-7}$ SI) at University of Bayreuth, Germany. For the samples from the Râmnicu Sărat section the magnetic susceptibility was measured with an AGICO MFK1-FA Kappabridge (sensitivity $\sim 2 \times 10^{-8}$ SI) using a magnetic field of 200 A/m and two frequencies: 976 Hz and 15616 Hz at University of Bucharest, Romania. All data were corrected for drift and for the effect of holder and sampling boxes (weak diamagnetism) and normalized to

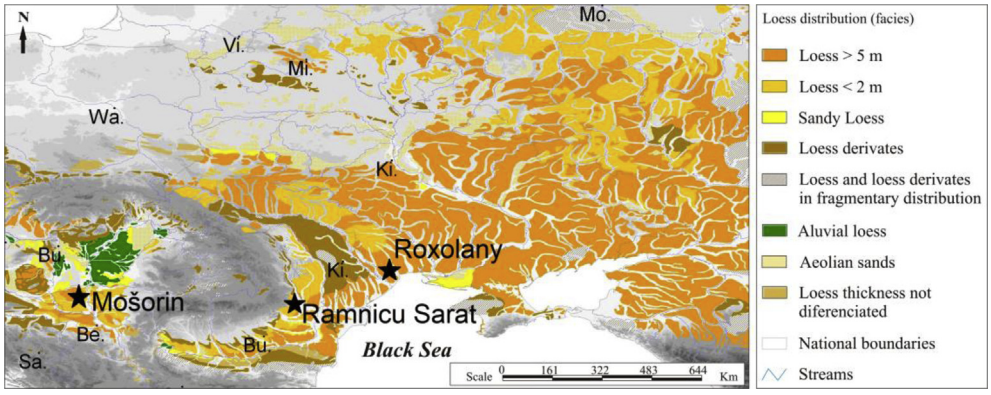

Fig. 1. Loess distribution in southeastern Europe (after Haase et al., 2007). The loess sites investigated in this study are indicated with filled stars. The acronyms indicate the major cities. Mo.: Moscow, Ki.: Kiev, Ki.: Kishnev, Bu.:Bucharest, Mi: Minsk, Vi.:Vilnius, Wa.: Warsaw, Bu.: Budapest, Be.: Belgrade, Sa.: Sarajevo.

mass. Frequency dependence of magnetic susceptibility was expressed as a mass-specific loss of susceptibility $\chi_{fd} = \chi_{lf} - \chi_{hf}$, where χ_{lf} and χ_{hf} are the magnetic susceptibility measured at low and high frequency, respectively (Dearing et al., 1996).

3.2. Optically stimulated luminescence dating

3.2.1. Sample preparation

In subdued red light in the laboratory, the material from each end of the samples was dried, finely milled and packet for gamma spectrometry measurements. Standard procedures were applied on the remaining core material in order to extract quartz grains with the following grain-sizes: 4–11 μm, 63–90 μm and 90–125 μm (where available) and polymineral fine (4–11 μm) grains. More details on sample preparation can be found in the Supplementary Material. The 4–11 μm quartz and polymineral fractions were mounted on aluminium disks from a suspension in acetone (2 mg/ml). Coarse (> 63 μm) quartz grains were then fixed using silicone oil onto 9.7 cm stainless steel disks.

3.2.2. Equivalent dose determination

Luminescence measurements have been carried out on standard Risø TL/OSL DA-20 readers (Thomsen et al., 2006). Quartz luminescence investigations were performed using the single-aliquot regenerative dose (SAR) protocol (Murray and Wintle, 2000, 2003). The luminescence signals were stimulated with blue light emitting diodes for 40 s at 125 °C. The net CW-OSL (optically stimulated luminescence) signal was selected from the first 0.308 s of the decay curve minus an early background subtracted from the 1.69–2.30 s interval. The OSL response to a fixed test dose of 17 Gy was used throughout the whole set of measurements to correct for sensitivity changes. At the end of each SAR cycle a high-temperature bleach for 40 s at 280 °C was performed by stimulation with blue diodes (Murray and Wintle, 2003). Equivalent doses have been measured on fine (4–11 μm) and coarser (63–90 μm and 90–125 μm if available) quartz extracts from Roxolany and Mošorin, while for Râmnicu Sărat only the 63–90 μm quartz fraction was investigated.

For the sake of consistency, feldspar infrared luminescence investigations were performed on 4–11 μm polymineral grains extracted from the Mošorin samples by applying the post-IR $IRSL_{290}$ protocol (Thiel et al., 2011). The samples were preheated to 320 °C for 60 s and exposed to IR diodes for 200 s at 50 °C to allow recombination of near-neighbour trap and centre pairs. The post IR IRSL signal was stimulated with IR LEDs at 290 °C for 200 s. The net signal was integrated from the initial ~2.3 s of stimulation, less a background from the last 20 s. A test dose of 14 Gy was used to monitor for the sensitivity changes and a high-temperature bleach for 100 s at 325 °C was performed at the end of each cycle in order to remove residual charge. Residual doses were determined on five natural aliquots from samples MVS 3, 4, 7 after 4 h bleaching in a SOL2 solar simulator (Thiel et al., 2011; Buylaert et al., 2012). An average residual dose was calculated from the bleached aliquots and was subtracted from the equivalent doses obtained for the rest of the samples.

Standard performance tests (recycling and recuperation) (Murray and Wintle, 2003) tests have been included in every measurement. The purity of the quartz extracts was confirmed by OSL IR depletion tests (Duller, 2003) on all aliquots measured. Recycling ratios and OSL IR depletion ratios within a maximum deviation of 10% from unity were considered suitable, as was a recuperation signal amounting to less than 2% of the natural signal.

3.2.3. Dosimetry

The annual dose rates were calculated based on radionuclide specific activities measured by means of high resolution gamma spectrometry using a well-type HPGe detector. Samples have been stored for at least one month in order to achieve ^{226}Ra-^{222}Rn equilibrium. The surveyed gamma lines in the ^{238}U series were 63.29 keV (^{234}Th), 92.38 keV (^{234}Th), 92.8 keV (^{234}Th), 351 keV (^{214}Pb), 295 keV (^{214}Pb), 609.3 keV (^{214}Bi) and 46.5 keV (^{210}Pb). The used gamma lines from the ^{232}Th series were 338 keV (^{228}Ac), 911 keV (^{228}Ac), 238 keV (^{212}Pb), 583 keV (^{208}Tl). The 1461 keV peak was used to determine the specific activity of ^{40}K. In order to assess whether the radioactive equilibrium prevailed at the investigated sites daughter to parent ratios (^{226}Ra:^{234}Th, ^{212}Pb:^{228}Ac) have been calculated for the two radioactive series (Fig. S5 inset and Fig. S6).

The dose rates were derived based on the conversion factors tabulated by Adamiec and Aitken (1998). The beta attenuation and etching factor for 63–90 μm and 90–125 μm was assumed to be 0.94 ± 0.05 and 0.92 ± 0.05, respectively (Mejdahl, 1979). The alpha efficiency value was taken as 0.04 ± 0.02 for quartz and as 0.08 ± 0.02 for polymineral fine-grains (Rees-Jones, 1995). The time averaged water content was taken as the difference between the natural 'as found' weight and the oven-dried weight of the material with a relative error of 25%. The total dose rate includes the external contribution from beta and gamma radiation (additionally alpha radiation contributions for the 4–11 μm grains), as well as the cosmic ray contribution. The cosmic ray dose rate was estimated for each sample as a function of depth, altitude and geomagnetic latitude (Prescott and Hutton, 1994). The internal dose rate contribution for the coarse quartz fraction was assumed to be 0.010 ± 0.002 Gy/ka (Vandenberghe et al., 2008).

4. Results and discussion

4.1. Luminescence properties and equivalent doses

The decay of the luminescence emission with stimulation time is represented in insets of Fig. S4 a, b, c. The quartz luminescence signals from all samples displayed a sharp decay down to 20% of the initial signal within the first second of stimulation. The fast decay rate is comparable to that displayed by the calibration quartz luminescence signal (insets Fig. S4 b and c). The growth of the OSL signal is best fitted by the sum of two saturating exponential functions using the Origin 8 program:

$$I(D) = I_0 + A\left(1 - \exp\left(-\frac{D}{D_{01}}\right)\right) + B\left(1 - \exp\left(-\frac{D}{D_{02}}\right)\right)$$

where I is the intensity of the signal for a given dose D, I_0 is the intercept, A and B are the saturation characteristics of the two exponential components and D_{01}, D_{02} are the doses that characterize the onset of saturation of each exponential function, also named characteristic doses in the literature. Representative dose response curves are shown in Fig. S4.

We have investigated the dependence of the equivalent doses on the heat treatments using a selection of quartz samples. Five aliquots were measured for each temperature combination. The preheat following the natural or regenerative dose was held for 10 s. Prior to test dose signal read out the aliquots were heated up to the cutheat temperature and immediately cooled. Fig. 2 shows that in neither case is there any systematic variation in D_e with preheat temperature in the 200–240 °C interval.

We have checked whether the SAR protocol can successfully recover a known irradiation dose given prior to any thermal treatment by employing the dose recovery test (Wallinga et al., 2000; Murray and Wintle, 2003). Sets of five natural aliquots were prepared from 63–90 μm quartz samples (ROX 1.4, RS 90, RS 100, RS 120, RS 150, RS 160, MVS 6 and MVS 9) and 4–11 μm quartz samples (ROX 1.4, MVS 6 and MVS 9). Their natural signal was bleached by exposure to two blue light emitting diode stimulations of 100 s at room temperature with an intervening pause of 10000 s. The aliquots then received beta irradiation doses that approximated their equivalent doses. These surrogate doses were then measured using the SAR protocol. The Roxolany and

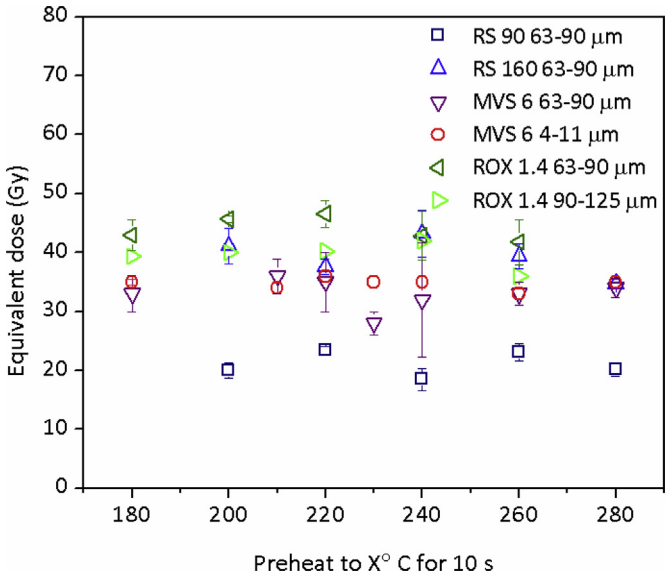

Fig. 2. Equivalent dose variations with the preheat temperature (heating treatment applied before natural and regenerative signal readout). The cutheat (heating of sample before the test dose signal readout) used for Roxolany and Râmnicu Sărat sample varied from 160 °C for preheats of 180 °C, to 180 °C for preheats between 200 and 220 °C, to 220 °C for preheats higher than 240 °C. For the Mošorin Veliki Surduk samples, a cutheat of 160 °C was used throughout all measurements.

Râmnicu Sărat quartz samples were heated at 220 °C for 10 s before the natural or regenerative signal readout and to 180 °C and immediately cooled before stimulating the luminescence signal induced by the test dose. For the Mošorin samples, a preheat/cutheat combination of 200 °C/160 °C was chosen. As seen in Fig. 3 a, for the quartz samples, the SAR protocol accurately recovered the given doses within a 10% deviation from unity. Consequently, a preheat temperature of 220 °C for 10 s and a cutheat to 180 °C were employed throughout the SAR protocol for equivalent doses determination of Roxolany and Râmnicu Sărat quartz samples and a preheat/cutheat combination of 200 °C/160 °C for the Mošorin quartz samples. The dose recovery test was also applied on five polymineral fine grained aliquots from sample MVS 3. They were bleached in the solar simulator for 24 h to reduce the natural signal to a low level. A 40 Gy beta dose was then delivered and measured using the post-IR $IRSL_{290}$ protocol described above. From the recovered dose a residual dose of 7.0 ± 0.4 Gy (determined after exposure for 4 h in the solar simulator) was subtracted. The post-IR $IRSL_{290}$ overestimated the given dose yielding a dose recovery ratio of 1.23 ± 0.04, while the recycling and recuperation test were successfully passed for all measured aliquots. These results show that the quartz luminescence behavior of the investigated samples is appropriate for the measurement procedures applied. In contrast, the dose recovery results of the post-IR $IRSL_{290}$ protocol applied to polymineral fine-grains is not satisfactory.

The equivalent doses and the number of aliquots used are given in Tables S1–3. The recycling, OSL IR depletion and recuperation ratio are displayed in Fig. 3 b. Relative standard deviation (RSD) and overdispersion (OD) in individual multigrain equivalent dose data have been calculated for each sample (Fig. S7). They are generally below 20% with the exception of the uppermost soil samples, probably disturbed by agricultural activities, and don't differentiate the loess from the soil samples. Such results are consistent with those on undisturbed loess samples reported in the literature (Lai and Wintle, 2006; Buylaert et al., 2008; Timar-Gabor et al., 2011, 2015). This ensures us that significant post-depositional mixing is unlikely to be an issue in the investigated samples.

As it can be seen from Table S3, the equivalent doses obtained on polymineral grains are systematically higher, sometimes beyond 100% of those obtained on fine grained quartz. This might be partly explained by the existence of unbleachable residuals of the post-IR IRSL signal. The post-IR $IRSL_{290}$ signal is evicted from deeper, harder to bleach, traps in feldspars compared to the fast component sampled from quartz OSL signal (Thiel et al., 2011). The residual doses determined for the post-IR IRSL signal from polymineral fine-grains after 4h SOL2 bleaching are large (up to 19 Gy, Table S3). Similar residuals have been observed for modern and young loess from China and Europe (Buylaert et al., 2011; Thiel et al., 2011). Moreover, the overestimated dose recovery test results using the post-IR $IRSL_{290}$ protocol might explain better the overestimation of the feldspar equivalent dose results. This inaccurate dose recovery testifies to the poor suitability of the post-IR $IRSL_{290}$ protocol for the investigated samples.

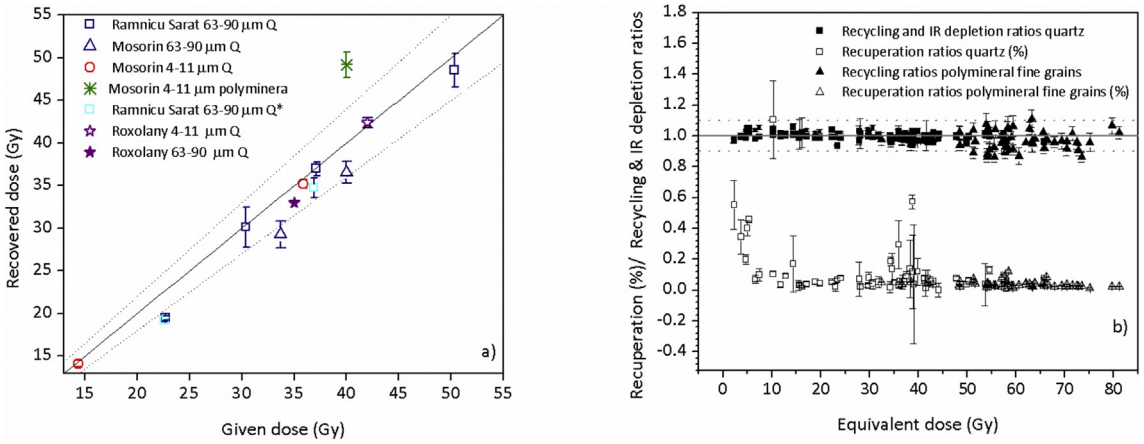

Fig. 3. a) Dose recovery test results. The given irradiation doses were chosen to match the equivalent dose of each sample. The thermal treatment of the Roxolany and Râmnicu Sărat quartz samples involved a 10 s preheat at 220 °C and a cutheat of 180 °C. Dose recovery test was repeated on two samples from Râmnicu Sărat using a 10 s preheat at 180 °C and a cutheat of 160 °C and are denoted with *. The fine and coarse quartz samples from Mošorin Veliki Surduk were measured using a 200 °C preheat for 10 s in combination with a cutheat of 160 °C. The polymineral fine grain sample from Mošorin Veliki Surduk was measured using the post-IR $IRSL_{290}$ protocol (Buylaert et al., 2012). Before laboratory irradiation, the aliquots were bleached in the solar simulator for 24 h to ensure the removal of the natural signal. The solid line indicates the ideal 1:1 dose recovery ratio while the dotted lines bracket a 10% variation from unity. **b) Intrinsic performance test results of the SAR protocol** applied on all quartz samples are given with filled and open squares. The general behavior of the polymineral fine grains in the post-IR $IRSL_{290}$ protocol are represented with filled and open triangles. Each point represents the average ratio obtained for each grain size fraction of each sample presented in this study. The solid line indicates the ideal recycling and IR depletion ratios, whereas the dotted lines bracket the accepted 10% deviation from unity.

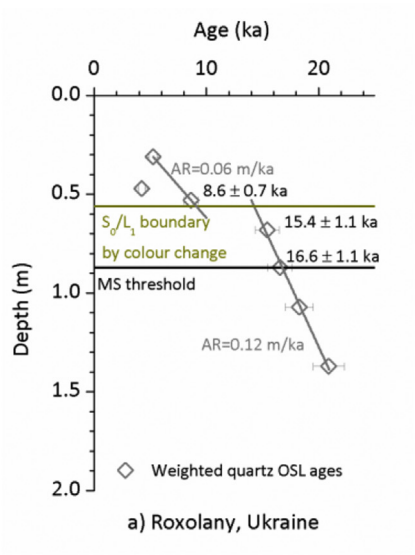

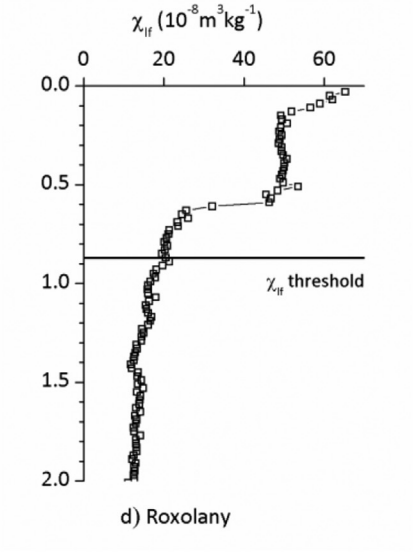

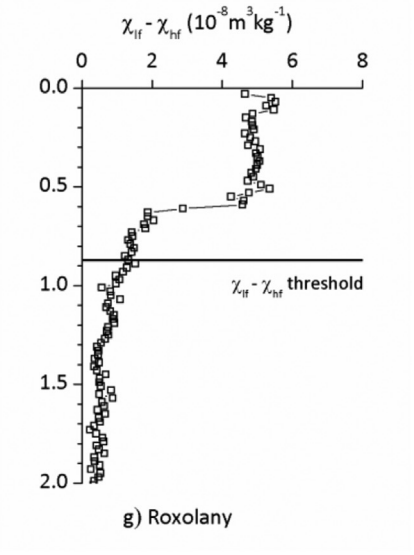

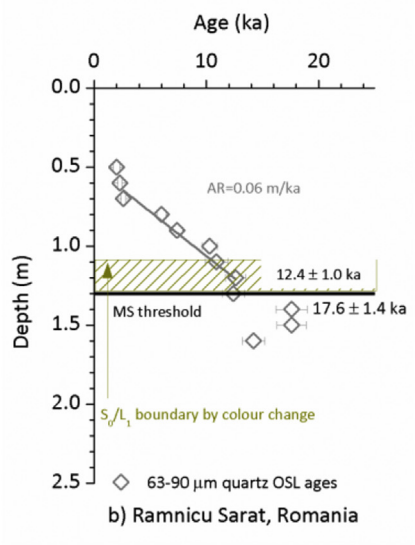

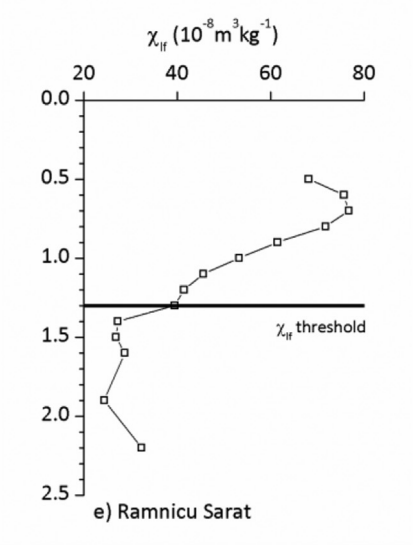

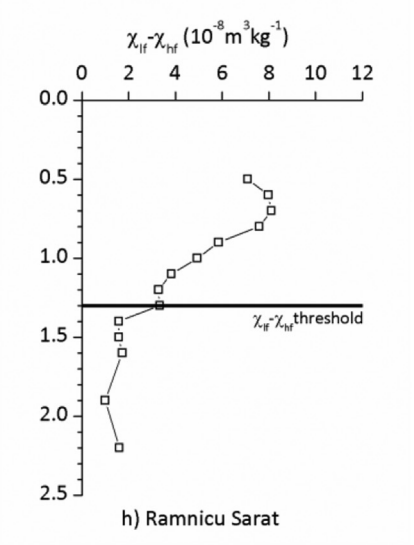

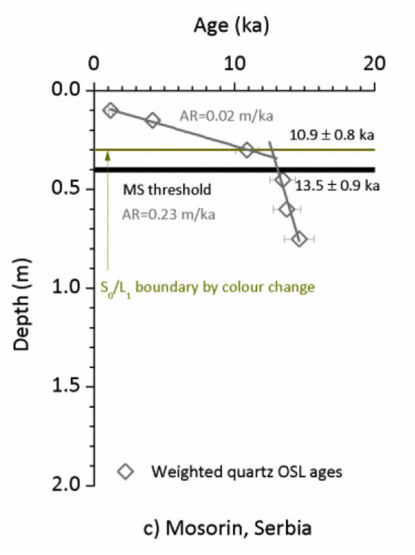

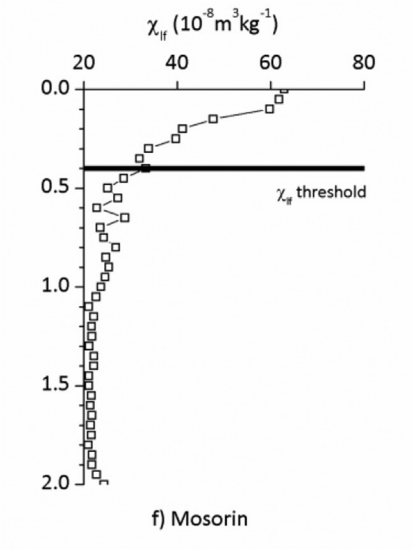

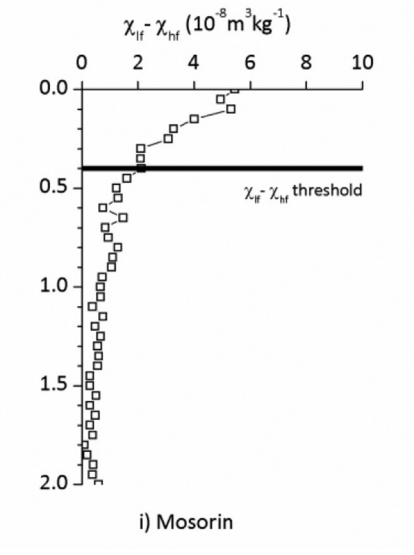

(caption on next page)

Fig. 4. a-c) Quartz OSL ages displayed as function of depth in all three sites investigated. For Roxolany, weighted average ages have been calculated according to Aitken (1985) using the ages yielded by 4–11 μm, 63–90 μm and 90–125 μm quartz. The Râmnicu Sărat ages are obtained on the 63–90 μm quartz fraction. For Mošorin Veliki Surduk, the weighted average ages have been calculated using the ages obtained on 4–11 μm and 63–90 μm quartz. Sediment accumulation rates (AR) have been calculated using linear regression of the OSL ages with depth (**a-c**). Information regarding the threshold in the MS record are given in text. The S0/L1 boundary identified in the field is also shown for reference. **d-f)** Low frequency magnetic susceptibility curves. **g-i)** Frequency dependence magnetic susceptibility curves expressed as a mass-specific loss of susceptibility $\chi_{fd} = \chi_{lf} - \chi_{hf}$, where χ_{lf} and χ_{hf} are the MS measured at low and high frequency, respectively (Dearing et al., 1996).

4.1.1. OSL ages

The relevant information on the total annual dose rates is listed along with the OSL ages in Tables S1–3. Quantification of the radon loss was not possible due to large uncertainties and systematic severe underestimations for ^{210}Pb measurements. However, a worst-case scenario in case of radioactive disequilibrium (considering significant ^{222}Rn loss) is presented in Fig. S8. The OSL ages are generally correlated within error limits with those calculated assuming radioactive equilibrium. Based on this argument, throughout this study we discuss the OSL ages calculated assuming radioactive equilibrium in the uranium series.

Uncertainties on the ages were calculated following Aitken and Alldred (1972). The systematic errors are dominated by the uncertainties associated with the estimates for time-averaged water content, alpha irradiation efficiency in the case of fine grains, and beta attenuation factors. The relative systematic errors on the fine-grained quartz ages amount to 8–9%, while in the case of coarse fractions they are around 6%. The relative random errors for fine material are below 5%, while for the 63–90 μm and 90–125 μm fractions they are generally less than 9%.

The OSL results obtained on different quartz extracts provide coeval age ranges and are internally consistent. Therefore, weighted average fine and coarse quartz ages were calculated for Mošorin and Roxolany samples following Aitken (1985, Appendix B). The post-IR $IRSL_{290}$ ages significantly overestimate the quartz data and are not considered further.

4.2. Dating of the magnetic susceptibility threshold

The rock magnetic data of loess-paleosol samples, such as low-field magnetic susceptibility (χ_{lf}) and its dependence on the frequency of the applied field (χ_{fd}) are generally reliable indicators for the intensity of soil forming processes, as well as chemical weathering of primary loess; the latter being a proxy for the exclusively pedogenetically formed fraction of ferrimagnetic minerals (Maher et al., 2003). As the intensity of pedogenesis is controlled mainly by hydroclimate variability, the trends in χ_{lf} and χ_{fd} are often regarded as reliable paleoclimate proxies (e.g. Buggle et al., 2014). As such, they were commonly employed in deriving tie-points both for the direct linking of loess-paleosol sequences with benthic δ^{18}O stacks and for deriving age-models, especially over orbital time-scales (e.g. Necula and Panaiotu, 2008; Zeeden et al., 2018).

Most of the LPS sections from the Danube Basin and the Black Sea cost (e.g. Marković et al., 2015; Necula et al., 2015) and also from China (e.g. Dong et al., 2015) show a gradual increase of magnetic susceptibility from the Last Glacial Maximum (LGM) to the Holocene. This behavior is similar to the benthic δ^{18}O changes (Stern and Lisiecki, 2014) observed over the most recent deglaciation (Termination 1). Following this, we have defined the threshold of the transition from the LGM to Holocene by adopting an approach similar to the one used by Stern and Lisiecki (2014). We have constrained the onset of the transition at the depth where both χ_{lf} and χ_{fd} values increase significantly and continuously compared to those values that characterize the last glacial loess (or more specifically the LGM loess).

At Roxolany the minimum χ_{lf} and χ_{fd} values lie around 137 cm. An OSL age of 21 ± 1.4 ka corresponds to this depth indicating that the loess has been deposited during the LGM (Fig. 4a). From this point up there is a gradual increase of both χ_{lf} and χ_{fd} until after 15.4 ± 1.1 ka, when a large and rapid jump in the magnetic signal is identified. However, the values start to increase significantly compared to those characteristic of the LGM around 87 cm. An OSL age of 16.6 ± 1.1 ka has been determined for the loess at this depth. We place the threshold in the magnetic susceptibility variation at 87 cm (Fig. 4a) and we interpret it as likely reflecting the onset of soil formation during the Pleistocene to Holocene transition (ie, the Late Glacial) at the Roxolany section. Based on linear regression of OSL ages with depth it seems that during the transition from the LGM to the Holocene the sedimentation rate seems to be constant. The nature and significance of the rapid increase observed in magnetic susceptibility values between 15.4 ± 1.1 ka and 8.6 ± 0.7 ka needs further investigation.

Both χ_{lf} and χ_{fd} at Râmnicu Sărat section display low values in the last glacial loess up to 140 cm depth (Fig. 4e, h). The OSL sample collected at this depth was dated to 17.6 ± 1.4 ka (Fig. 4b). A steady increase in the magnetic parameters is recorded between 120 cm and 70 cm. This pattern is similar to the one observed on a parallel section sampled at a higher resolution (5 cm) in the same place (Fig. S9, Dimofte, 2012). Thus, the threshold of the increase of magnetic susceptibility can be placed between 140 and 130 cm, taking place along a 10 cm interval at the bottom of the transitional zone from L1 to S0 observed in the field. The samples collected at these depths yielded OSL ages of 17.6 ± 1.4 ka and 12.4 ± 1.0 ka (Fig. 4b). The sedimentation rate after 12 ka is relative constant during the period of gradual increase of magnetic susceptibility.

At Mošorin, both χ_{lf} and χ_{fd} values increase significantly compared to those in the last glacial loess immediately above 45 cm (Fig. 4f, i). The OSL sample collected at this the depth was dated to 13.5 ± 0.9 ka (Fig. 4c). From this depth and upwards, the χ_{lf} and χ_{fd} values increase continuously. By carrying out a regression of OSL ages with the depth down the section, a significant reduction in sedimentation rate can be also noticed around 13.5 ± 0.9 ka (Fig. 4c).

5. Conclusion

SAR-OSL dating of 4–11 μm, 63–90 μm and 90–125 μm quartz provided consistent ages for the transition from the last glacial loess to the modern soil in three loess-paleosol sites in southeastern Europe, while the post-IR $IRSL_{290}$ protocol applied to polymineral fine-grains is not suitable for accurate dating of these young samples.

We have associated the L1/S0 transition with the threshold point at which the magnetic susceptibility enhancement becomes significantly higher than in the last glacial loess. Thus, the magnetic susceptibility threshold was placed around 16.6 ± 1.1 ka at Roxolany, 13.5 ± 0.9 ka at Mošorin and between 17.6 ± 1.4 ka and 12.4 ± 1.0 ka at Râmnicu Sărat. Due to the limitations imposed by the nature of the L1/S0 in the investigated sites, it is not possible to define a universal threshold in the magnetic susceptibility data that is valid for all the investigated sections and further investigations are in progress in other sites. However, the behavior of magnetic susceptibility reflects a gradual transition from the Last Glacial towards the Holocene. These results indicate that the onset of the magnetic signal enhancement produced by pedogenesis in the investigated sites in SE Europe started around Termination 1 (~17 ka in the North Atlantic) as observed in radiocarbon-dated regional benthic δ^{18}O stacks (Stern and Lisiecki, 2014), but before the stratigraphic Pleistocene/Holocene transition dated at 11.7 ka in ice core records.

Acknowledgements

This project has received funding from the European Research Council (ERC) under the European Union's Horizon 2020 research and innovation programme ERC-2015-STG (grant agreement No [678106] awarded to Alida Timar-Gabor).

Appendix A. Supplementary data

Supplementary data related to this article can be found at https://doi.org/10.1016/j.quageo.2018.07.011.

References

Adamiec, G., Aitken, M.J., 1998. Dose-rate conversion factors: update. Ancient TL 16, 37–50.

Aitken, M.J., 1985. Thermoluminescence Dating. Academic Press, London.

Aitken, M.J., Alldred, J.C., 1972. The assessment of error limits in thermoluminescent dating. Archaeometry 14, 257–267.

Blockley, S.P.E., Lane, C.S., Hardiman, M., Rasmussen, S.O., Seierstad, I.K., Steffensen, J.P., Svensson, A., Lotter, A.F., Turney, C.S.M., Bronk Ramsey, C., 2012. Synchronisation of palaeoenvironmental records over the last 60,000 years, and an extended INTIMATE event stratigraphy to 48,000 b2k. Quat. Sci. Rev. 36, 2–10.

Buggle, B., Hambach, U., Müller, K., Zöller, L., Marković, S.B., Glaser, B., 2014. Iron mineralogical proxies and Quaternary climate change in SE-European loess-paleosol sequences. Catena 117, 4–22.

Buylaert, J.P., Murray, A.S., Vandenberghe, D., Vriend, M., De Corte, F., Van den haute, P., 2008. Optical dating of Chinese loess using sand-sized quartz: establishing a time frame for Late Pleistocene climate changes in the western part of the Chinese Loess Plateau. Quat. Geochronol. 3, 99–113.

Buylaert, J.-P., Thiel, C., Murray, A.S., Vandenberghe, D.A.G., Yi, S., Lu, H., 2011. IRSL and post-IR IRSL residual doses recorded in modern dust samples from the Chinese Loess Plateau. Geochronometria 38 (4), 432–440.

Buylaert, J.-P., Jain, M., Murray, A.S., Thomsen, K.J., Thiel, C., Sohbati, R., 2012. A robust feldspar luminescence dating method for Middle and Late Pleistocene sediments. Boreas 41, 435–451.

Dearing, J.A., Dann, R.J.L., Hay, K., Lees, J.A., Loveland, P.J., Maher, B.A., O'Grady, K., 1996. Frequency-dependent susceptibility measurements of environmental materials. Geophys. J. Int. 124, 228–240.

Dimofte, D., 2012. Schimbări climatice cuaternare înregistrate în depozite sedimentare deduse prin analize mineralogice, granulometrice, geochimice şi magnetice pe secţiuni de loess-paleosol din România Climatic fluctuation recorded by loess-paleosol deposits from Romania using mineralogical, granulometric, geochemical and magnetic data. PhD thesis. University of Bucharest 165 pp (in Romanian).

Dong, Y., Wu, N., Li, F., Huang, L., Wen, W., 2015. Time-transgressive nature of the magnetic susceptibility record across the Chinese Loess Plateau at the Pleistocene/Holocene transition. PLoS One 10 (7), e0133541. https://doi.org/10.1371/journal.pone.0133541.

Duller, G.A.T., 2003. Distinguishing quartz and feldspar in single grain luminescence measurements. Radiat. Meas. 37, 161–165.

Govin, A., Capron, E., Tzedakis, P.C., Verheyden, S., Ghaleb, B., Hillaire-Marcel, C., St-Onge, G., Stoner, J.S., Bassinot, F., Bazin, L., Blunier, T., Combourieu-Nebout, N., El Ouahabi, A., Genty, D., Gersonde, R., Jimenez-Amat, P., Landais, A., Martrat, B., Masson-Delmotte, V., Parrenin, F., Seidenkrantz, M.S., Veres, D., Waelbroeck, C., Zahn, R., 2015. Sequence of events from the onset to the demise of the Last Interglacial: evaluating strengths and limitations of chronologies used in climatic archives. Quat. Sci. Rev. 129, 1–36.

Haase, D., Fink, J., Haase, G., Ruske, R., Pecsi, M., Richter, H., Altermann, M., Jäger, K.D., 2007. Loess in Europe - its spatial distribution based on a european loess map, scale 1:2,500,000. Quat. Sci. Rev. 26 (9–10), 1301–1312.

Lai, Z.-P., Wintle, A.G., 2006. Locating the boundary between the Pleistocene and the Holocene in Chinese loess using luminescence. Holocene 16 (6), 893–899.

Lisiecki, L.E., Raymo, M.E., 2005. A Pliocene-Pleistocene stack of 57 globally distributed benthic δ18O records. Paleoceanography 20https://doi.org/10.1029/2004PA001071. PA1003.

Maher, B.A., Yu, H.M., Roberts, H.M., Wintle, A.G., 2003. Holocene loess accumulation and soil development at the western edge of the Chinese Loess Plateau: implications for magnetic proxies of palaeorainfall. Quat. Sci. Rev. 22, 445–451.

Marković, S.B., Stevens, T., Kukla, G.J., Hambach, U., Fitzsimmons, K.E., Gibbard, P., Buggle, B., Zech, M., Guo, Z., Hao, Q., Wu, H., O'Hara Dhand, K., Smalley, I.J., Újvári, G., Sümegi, P., Timar-Gabor, A., Veres, D., Sirocko, F., Vasiljević, D.A., Jary, Z., Svensson, A., Jović, V., Lehmkuhl, F., Kovács, J., Svirčev, Z., 2015. Danube loess stratigraphy – towards a pan-European loess stratigraphic model. Earth Sci. Rev. 148, 228–258.

Mejdahl, V., 1979. Thermoluminescence dating: beta dose attenuation in quartz grains. Archaeometry 21, 61–72.

Murray, A.S., Wintle, A.G., 2000. Luminescence dating of quartz using an improved single-aliquot regenerative-dose protocol. Radiat. Meas. 32, 57–73.

Murray, A.S., Wintle, A.G., 2003. The single aliquot regenerative dose protocol: potential for improvements in reliability. Radiat. Meas. 37, 377–381.

Nawrocki, J., Gozhik, P., Łanczont, M., Pańczyk, M., Komar, M., Bogucki, A., Williams, I.S., Czupyt, Z., 2018. Palaeowind directions and sources of detrital material archived in the Roxolany loess section (southern Ukraine). Palaeogeogr. Palaeoclimatol. Palaeoecol. 496, 121–135.

Necula, C., Panaiotu, C., 2008. Application of dynamic programming to the dating of a loess paleosol sequence. Rom. Rep. Phys. 60, 157–171.

Necula, C., Dimofte, D., Panaiotu, C., 2015. Rock magnetism of a loess-paleosol sequence from the western Black Sea shore (Romania). Geophys. J. Int. 202, 1733–1748.

Perić, Z., Lagerbäck Adolphi, E., Stevens, T., Újvári, G., Zeeden, C., Buylaert, J.-P., Marković, S.B., Hambach, U., Fischer, P., Schmidt, C., Schulte, P., Huayu, L., Shuangwen, Y., Lehmkuhl, F., Obreht, I., Veres, D., Thiel, C., Frechen, M., Jain, M., Vött, A., Zöller, L., Gavrilov, M.B., 2018. Quartz OSL dating of late quaternary Chinese and Serbian loess: a cross Eurasian comparison of dust mass accumulation rates. Quat. Int. https://doi.org/10.1016/j.quaint.2018.01.010 (in press).

Prescott, J.R., Hutton, J.T., 1994. Cosmic ray contributions to dose rates for luminescence and ESR dating: large depths and long term variations. Radiat. Meas. 23, 497–500.

Rasmussen, S.O., Bigler, M., Blockley, S.P., Blunier, T., Buchardt, S.L., Clausen, H.B., Cvijanovic, I., Dahl-Jensen, D., Johnsen, S.J., Fischer, H., Gkinis, V., Guillevic, M., Hoek, W.Z., Lowe, J.J., Pedro, J.B., Popp, T., Seierstad, I.K., Steffensen, J.P., Svensson, A.M., Vallelonga, P., Vinther, B.M., Walker, M.J.C., Wheatley, J.J., Winstrup, M., 2014. A stratigraphic framework for abrupt climatic changes during the Last Glacial period based on three synchronized Greenland ice-core records: refining and extending the INTIMATE event stratigraphy. Quat. Sci. Rev. 106, 14–28.

Rees-Jones, J., 1995. Optical dating of young sediments using fine-grain quartz. Ancient TL 13, 9–13.

Roberts, H.M., 2008. The development and application of luminescence dating to loess deposits: a perspective on the past, present and future. Boreas 37, 483–507.

Stern, J.V., Lisiecki, L.E., 2014. Termination 1 timing in radiocarbon-dated regional benthic $\delta^{18}O$ stacks. Paleoceanography 29, 1127–1142.

Stevens, T., Marković, S.B., Zech, M., Hambach, U., Sümegi, P., 2011. Dust deposition and climate in the Carpathian Basin over an independently dated last glacial-interglacial cycle. Quat. Sci. Rev. 30, 662–681.

Stevens, T., Buylaert, J.-P., Thiel, C., Újvári, G., Yi, S., Murray, A.S., Frechen, M., Lu, H., 2018. Ice-volume-forced erosion of the Chinese Loess Plateau global Quaternary stratotype site. Nat. Commun. 9 (983).

Svensson, A., Andersen, K.K., Bigler, M., Clausen, H.B., Dahl-Jensen, D., Davies, S.M., Johnsen, S.J., Muscheler, R., Parrenin, F., Rasmussen, S.O., Röthlisberger, R., Seierstad, I., Steffensen, J.P., Vinther, B.M., 2008. A 60 000 year Greenland stratigraphic ice core chronology. Clim. Past 4, 47–57.

Thiel, C., Buylaert, J.-P., Murray, A., Terhorst, B., Hofer, I., Tsukamoto, S., Frechen, M., 2011. Luminescence dating of the Stratzing loess profile (Austria) – testing the potential of an elevated temperature post-IR IRSL protocol. Quat. Int. 234, 23–31.

Thomsen, K.J., Bøtter-Jensen, L., Denby, P.M., Moska, P., Murray, A.S., 2006. Developments in luminescence measurement techniques. Radiat. Meas. 41, 768–773.

Timar-Gabor, A., Vandenberghe, D.A.G., Vasiliniuc, S., Panaoitu, C.E., Panaiotu, C.G., Dimofte, D., Cosma, C., 2011. Optical dating of Romanian loess: a comparison between silt-sized and sand-sized quartz. Quat. Int. 240, 62–70.

Timar-Gabor, A., Constantin, D., Marković, S.B., Jain, M., 2015. Extending the area of investigation of fine versus coarse quartz optical ages from the Lower Danube to the Carpathian Basin. Quat. Int. 388, 168–176.

Vandenberghe, D.A.G., De Corte, F., Buylaert, J.-P., Kučera, J., Van den haute, P., 2008. On the internal radioactivity in quartz. Radiat. Meas. 43, 771–775.

Veres, D., Bazin, L., Landais, A., Toyé Mahamadou Kele, H., Lemieux-Dudon, B., Parrenin, F., Martinerie, P., Blayo, E., Blunier, T., Capron, E., Chappellaz, J., Rasmussen, S.O., Severi, M., Svensson, A., Vinther, B., Wolff, E.W., 2013. The Antarctic ice core chronology (AICC2012): an optimized multi-parameter and multi-site dating approach for the last 120 thousand years. Clim. Past 9, 1733–1748.

Wallinga, J., Murray, A.S., Wintle, A.G., 2000. The single aliquot regenerative-dose (SAR) protocol applied to coarse-grain feldspar. Radiat. Meas. 32, 529–533.

Zeeden, C., Hambach, U., Obreht, I., Hao, Q., Abels, H.A., Veres, D., Lehmkuhl, F., Gavrilov, M.B., Marković, S.B., 2018. Patterns and timing of loess-paleosol transitions in Eurasia: constraints for paleoclimate studies. Global Planet. Change 162, 1–7.